15.9 % Organic Tandem Solar Cell with Extended Near-infrared Absorption

Xinjing Huang[1*], Bangjin Sun[2*], Yongxi Li[3], Chao Jiang[2], Dejiu Fan[3], Jian Fan[2+] and Stephen R. Forrest[1,3,4+]

1. Applied Physics Program, University of Michigan, Ann Arbor, MI 48109, USA

2. Institute of Functional Nano & Soft Materials, Jiangsu Key Laboratory for Carbon-Based Functional Materials & Devices, Soochow University, Suzhou, Jiangsu 215123, China

3. Department of Electrical Engineering and Computer Science, University of Michigan, Ann Arbor, MI 48109, USA

4. Department of Physics, and Material Science and Engineering, University of Michigan, Ann Arbor, MI 48109, USA

Abstract

Stacking single-junction organic solar cells is effective in increasing the power conversion efficiency (*PCE*) by reducing the thermalization loss and increasing the open circuit voltage. Recent developments of non-fullerene acceptors (NFAs) offer a range of materials whose energy gaps are suited for absorbing relatively narrow slices of the solar spectrum, thus easing requirements for current balance between sub-elements in the multijunction stacks. Here, we demonstrate a solution-processed tandem organic solar cell comprising a binary, visible-absorbing sub-cell and a ternary near-infrared (NIR) absorbing sub-cell. The ternary NIR sub-cell utilizes a narrow energy gap NFA acceptor that enables a broadened and increased absorption compared to a binary NIR sub-cell. An isopropanol surface treatment is developed to connect the hydrophilic-hydrophobic surfaces in the charge recombination zone (CRZ) located between the sub-cells. The

PLEASE CITE THIS ARTICLE AS DOI: 10.1063/5.0005172

nearly optically and electrically lossless CRZ combined with an anti-reflection coating results in a tandem OPV with *PCE* = 15.9 ± 0.2 % under AM 1.5G simulated illumination.

*: These authors contributed equally to this work.

+ Corresponding authors: Stephen Forrest, stevefor@umich.edu: Jian Fan, mailto:jianfan@suda.edu.cn

Organic photovoltaics (OPVs) are considered a promising means for solar energy harvesting due to their potential for low-cost, lightweight, transparency and flexibility.[1–4] By stacking wide and narrow energy gap cells into multijunction devices, the power conversion efficiency (*PCE*) can exceed the thermodynamic limit of single-junction devices due to their broader absorption spectral range with less thermalization losses and increased open circuit voltage.[5–10] Solution processed non-fullerene acceptors (NFAs) based on conjugated thiophene backbones have also provided a variety of molecules with spectral coverage useful for achieving current balance in multijunction solar cells while being compatible with a diversity of donor molecules.[11–14] In this work, we demonstrate a high efficiency tandem OPV structure that comprises one binary and one ternary solution-processed sub-cell. The development of near-infrared (NIR) absorbing NFA molecules with long wavelength (>1000 nm) cutoffs is critical to achieving a high *PCE*.[8,15–19] Here, we utilize a narrow energy gap NFA BEIT-4F that absorbs at wavelengths up to 1050 nm when combined with the donor, PCE-10, which enables the tandem solar cell to achieve broad spectral coverage from the blue to the NIR. We introduce a surface treatment with isopropanol to improve wetting without the need to add surfactant into the poly(3,4-ethylenedioxythiophene): poly(styrenesulfonate) (PEDOT:PSS) in the charge recombination zone (CRZ). The tandem cell device achieves *PCE* = 15.2 ± 0.2 % under AM 1.5G simulated illumination. An anti-reflection coating (ARC) deposited on the glass substrate increases the efficiency to 15.9 ± 0.2 %.

For the visible-absorbing sub-cell, we employ a wide energy gap NFA SFT8-4F combined with the polymer donor, PM6 (See Supplementary Information (SI) for detailed information of the molecules employed in the active regions of the sub-cells). Figure 1(a) presents the normalized

thin film absorption spectra of these two molecules. As shown, the absorption of SFT8-4F peaks at 750 nm, after which it decreases rapidly.

The ternary NIR absorbing sub-cell comprises a single donor PCE-10 and two acceptors BT-CIC and BEIT-4F. N-annulated perylene and dithienopicenocarbazole-based derivatives have been applied in efficient dye-sensitized and organic solar cells due to their planar frameworks and electron-donating capabilities.[16,20–22] The strong electron-donating motif dithienopicenocarbazole was incorporated into the BEIT-4F molecule to shift its absorption into the NIR, which is complementary to the absorption of SFT8-4F. As shown in the thin film absorption spectra in Fig. 1(b), the narrow energy gap NFA BEIT-4F absorption spectrum is 50 nm red-shifted compared to BT-CIC.

To systematically study the photogeneration mechanism in the ternary blends, we investigated their electronic states. Figure 2(a) presents the photoluminescence (PL) spectra of the ternary PCE-10:BT-CIC:BEIT-4F active region of the NIR sub-cell at different blend ratios. The PCE-10:BT-CIC binary exhibits the 0-0 transition peak of PCE-10 at 1.73 ± 0.01 eV, and for BT-CIC, at 1.39 ± 0.01 eV. The PCE-10:BEIT-4F binary and all ternary mixtures at different blend ratios have a BEIT-4F 0-0 transition at 1.32 ± 0.01 eV. In the ternary mixtures, excitons generated on BT-CIC rapidly transfer to BEIT-4F, which accounts for the absence of BT-CIC exciton peak in the PL spectra. Thus, the excited states in the ternary blends are not influenced by the mixture composition. Figure 2(b) shows the electroluminescence (EL) spectrum of PCE-10:BT-CIC binary blend. The spectrum comprises a BT-CIC exciton peak at 1.37 ± 0.02 eV and a PCE-10:BT-CIC charge transfer (CT) peak at 1.10 ± 0.02 eV. In Fig. 2(c) the EL spectrum of PCE-10:BEIT-4F binary

blend is fit with a BEIT-4F exciton peak at 1.30 ± 0.02 eV and a PCE-10:BEIT-4F CT peak at 1.15 ± 0.02 eV. The small energy offset between the highest occupied molecular orbitals (HOMO) of PCE-10 and BEIT-4F gives rise to hole transfer from the PCE-10 to the BEIT-4F HOMO. Hence, there is a prominent BEIT-4F exciton peak in the EL spectrum. Figure 2(d) presents the EL spectrum of a PCE-10:BT-CIC:BEIT-4F (1:1.25:0.5, w/w/w) ternary blend, which comprises BEIT-4F, PCE-10:BT-CIC CT and PCE-10:BEIT-4F CT exciton peaks, which are the same as those in the binaries. A similar fitting procedure is applied to this ternary system with different acceptor blend ratios. The spectral features fit well with the electronic states of the binaries. With these results, we infer that the ternary OPV operates as the combination of two, parallel-connected binary heterojunctions.[23]

The current density-voltage (*J-V*) characteristics and external quantum efficiency (*EQE*) spectra of ternary devices with different blend ratios are shown in Fig. 3(a) and 3(b), with detailed device performance data listed in Table 1. Compared to PCE-10:BT-CIC, the PCE-10:BEIT-4F binary OPV shows broader *EQE* spectrum that absorbs up to 1050 nm, a higher open-circuit voltage (V_{OC}) = 0.754 V ± 0.005 V vs. 0.695 V ± 0.004 V and a lower fill factor (*FF*) = 0.56 ± 0.01 vs. 0.71 ± 0.01. Consistent with the two binary junction model, adjusting the ratio of the two binary heterojunctions gives rise to *EQE*, V_{OC} and *FF* that fall between those of the binaries, and change monotonically with the blend ratio, as shown in Figs. 3(b) and 3(c).

To construct an optimized tandem OPV, the optical field was simulated to determine layer thicknesses and positions within the tandem cell required to achieve current balance. The lack of metal anode reflection of the PM6:SFT8-4F front sub-cell (i.e. the sub-cell adjacent to the

transparent ITO cathode) requires a thicker active layer to compensate for the reduced absorption, with the optimized structure shown in Fig. 4(a). The front sub-cell absorbs primarily between wavelengths of λ = 350 nm and 750 nm, whereas the back sub-cell which is adjacent to the reflective anode, absorbs primarily at λ > 750 nm. A nearly optically and electrically lossless CRZ was introduced between the sub-cells consisting of a polymer layer PEDOT:PSS sandwiched between a MoO_3 layer and a ZnO nanoparticle layer. To improve wetting between hydrophobic and hydrophilic surfaces, a thin layer of MoO_3 was thermal evaporated, and then precoated with a thin layer of isopropanol to initiate PEDOT:PSS deposition. This treatment significantly reduces the contact angle of PEDOT:PSS, and thus improves the fabrication yield (See SI Fig. S3).

Figure 4(b) and 4(c) presents the *J-V* characteristics and *EQE* spectra of the single-junction and tandem devices, with details listed in Table 2. The PM6:SFT8-4F (1:1.5, w/w, 80 nm) single junction device reaches PCE = 12.1 ± 0.3 % with J_{SC} = 18.4 ± 0.3 mA/cm^2, V_{OC} = 0.98 ± 0.01 V and FF = 0.67 ± 0.01. The trade-off between V_{OC} and FF in PCE-10:BT-CIC:BEIT-4F ternary NIR cell results in the highest PCE at a blend ratio 1:1.25:0.5 (w/w/w). Furthermore, the active layer was thermal annealed at 120 °C for 8 min to optimize the active layer morphology. The NIR absorbing device with 75 nm active layer thickness has PCE = 11.7 ± 0.3 % with absorption up to 1050 nm. This is 7% higher than the PCE of the PCE-10:BT-CIC binary device.

The optimized tandem OPV with 120 nm PM6:SFT8-4F front active layer and 90 nm PCE-10:BT-CIC:BEIT-4F back active layer exhibits J_{SC} = 13.5 ± 0.2 mA/cm^2, V_{OC} = 1.66 ± 0.01 V, FF = 0.68 ± 0.01 and PCE = 15.2 ± 0.2 % under simulated AM 1.5G illumination. To reduce the

optical loss, an ARC consisting of a 120 nm MgF_2 layer (index of refraction n_{MgF_2}=1.38±0.01) and a 130 nm low-refractive-index SiO_2 layer[24] (n_{SiO_2}=1.12±0.03) was deposited on the glass substrate, which reduced the reflection of glass substrate between 400 and 1000 nm for approximately 4%.[25] The tandem device with the ARC has an increased J_{SC} and a correspondingly increased *PCE*. As shown in Fig. 4(c), the tandem solar cell absorbs from 350 nm to 1050 nm. The reduced absorption of the front sub-cell is due to the lack of electrode reflection and back sub-cell absorption within the same wavelength region. This provides for current balance between sub-cells, along with a concomitant reduction in J_{SC} compared to that of the single junction PM6:SFT8-4F device. The integration of the *EQE* spectra gives a balanced front sub-cell J_{SC} = 14.2 mA/cm^2 and back sub-cell current of J_{SC} = 14.1 mA/cm^2. The tandem device with an ARC reaches *PCE* = 15.9 ± 0.2 %. Detailed performance parameters are listed in Table 2.

With rapid development in material synthesis, single-junction OPV has reached over 16% efficiency.[13,14] Multijunction solar cells can exceed the single-junction thermodynamic limit, which suggests that there is still room to improve the tandem OPV efficiency. Previously a double ternary-junction tandem cell with 17.3% PCE was demonstrated,[15] although the higher voltage of the tandem cell compared to the sum of the individual sub-cells was left unexplained. Nevertheless, results on high efficiency tandems points to their benefits of lower currents (and hence reduced series resistance losses), and their potential for higher *PCE* compared with single junction cells.

To conclude, we demonstrate a high efficiency tandem OPV structure with a NIR-absorbing PCE-10:BT-CIC:BEIT-4F ternary back sub-cell combined with a visible-absorbing binary PM6:SFT8-4F front sub-cell. The NIR-absorbing NFA BEIT-4F extends the absorption of the

back sub-cell to 1050 nm and results in current balance with the shorter wavelength absorbing binary front sub-cell. A nearly optically and electrically lossless CRZ comprising a hydrophilic PEDOT:PSS layer sandwiched between MoO_3 and ZnO nanoparticle layers is constructed using an isopropanol surface treatment. The tandem device on an ARC-coated glass substrate reaches a maximum $PCE = 15.9 \pm 0.2$ % under AM 1.5G simulated illumination.

Supplementary Information

See supplementary information for experimental details and contact angle measurement.

Data Availability Statement

The data that supports the findings of this study are available within the article and its supplementary material.

Acknowledgement

This work is supported in part by the U.S. Department of Energy's Office of Energy Efficiency and Renewable Energy (EERE) under Solar Energy Technologies Office (SETO) Agreement Number DE-EE0008561 (XH, YL), and by the Department of Navy, Office of Naval Research (ONR) under Award No. N00014-17-1-2211 (SRF, DF). This work is also supported by National Natural Science Foundation of China (No. 21871199), the Collaborative Innovation Centre of Suzhou Nano Science and Technology (Nano-CIC), Priority Academic Program Development of Jiangsu Higher Education Institutions (PAPD), and "111" Project of The State Administration of Foreign Experts Affairs of China (BS, CJ, JF).

Table I. Performance of PCE-10:BT-CIC:BEIT-4F Single-junction OPVs at Different Blend Ratios under Simulated AM 1.5G Illumination

PCE-10:BT-CIC:BEIT-4F[a]	J_{SC}[b] (mA/cm^2)	V_{OC} (V)	*FF*	*PCE* (%)
1:1.5:0	22.5 ± 0.2	0.695 ± 0.004	0.71 ± 0.01	11.0 ± 0.1
1:1.25:0.25	22.2 ± 0.3	0.703 ± 0.003	0.67 ± 0.01	10.5 ± 0.2
1:1.25:0.5	22.6 ± 0.2	0.715 ± 0.003	0.65 ± 0.01	10.9 ± 0.1
1:1.25:0.75	22.5 ± 0.2	0.726 ± 0.004	0.62 ± 0.01	10.4 ± 0.2
1:0:1.5	22.0 ± 0.3	0.754 ± 0.005	0.56 ± 0.01	9.3 ± 0.1

a: 4 mm^2 device area

b: The J_{SC} values are from the integrated *EQE* spectra

Table II. Discrete Sub-cells and Tandem Devices Performances under Simulated AM 1.5G Illumination

Device[a]	J_{SC}[c] (mA/cm^2)	V_{OC} (V)	*FF*	*PCE* (%)
PM6:SFT8-4F=1:1.5	18.4 ± 0.3	0.98 ± 0.01	0.67 ± 0.01	12.1 ± 0.3
PCE-10:BT-CIC:BEIT-4F = 1:1.25:0.5, TA[b]	24.3 ± 0.4	0.70 ± 0.01	0.68 ± 0.01	11.7 ± 0.3
Tandem w/o ARC	13.5 ± 0.2	1.66 ± 0.01	0.68 ± 0.01	15.2 ± 0.2
Tandem w/ ARC	14.1 ± 0.2	1.66 ± 0.01	0.68 ± 0.01	15.9 ± 0.2

a: 4 mm^2 device area

b: Thermal annealing at 120 °C

c: The J_{SC} values are from the integrated *EQE* spectra

References

[1] Y. Li, C. Ji, Y. Qu, X. Huang, S. Hou, C. Li, L. Liao, L.J. Guo, and S.R. Forrest, Adv. Mater. **31**, 1903173 (2019).

[2] Y. Li, G. Xu, C. Cui, and Y. Li, Adv. Energy Mater. **8**, 1 (2018).

[3] Y. Li, J.D. Lin, X. Che, Y. Qu, F. Liu, L.S. Liao, and S.R. Forrest, J. Am. Chem. Soc. **139**, 17114 (2017).

[4] B. Qu and S.R. Forrest, Appl. Phys. Lett. **113**, (2018).

[5] X. Che, Y. Li, Y. Qu, and S.R. Forrest, Nat. Energy **3**, 422 (2018).

[6] X. Che, X. Xiao, J.D. Zimmerman, D. Fan, and S.R. Forrest, Adv. Energy Mater. **4**, 1400568 (2014).

[7] J. Gilot, M.M. Wienk, and R.A.J. Janssen, Appl. Phys. Lett. **90**, 88 (2007).

[8] Y. Li, J.-D. Lin, X. Liu, Y. Qu, F.-P. Wu, F. Liu, Z.-Q. Jiang, and S.R. Forrest, Adv. Mater. **30**, 1804416 (2018).

[9] J. Gilot, M.M. Wienk, and R.A.J. Janssen, Adv. Mater. **22**, E67 (2010).

[10] D. Di Carlo Rasi and R.A.J. Janssen, Adv. Mater. **31**, 1806499 (2019).

[11] Y. Li, Acc. Chem. Res. **45**, 723 (2012).

[12] Q. Fan, T. Liu, W. Gao, Y. Xiao, J. Wu, W. Su, X. Guo, X. Lu, C. Yang, H. Yan, M. Zhang, and Y. Li, J. Mater. Chem. A **7**, 15404 (2019).

[13] J. Yuan, Y. Zhang, L. Zhou, G. Zhang, H.L. Yip, T.K. Lau, X. Lu, C. Zhu, H. Peng, P.A.

Johnson, M. Leclerc, Y. Cao, J. Ulanski, Y. Li, and Y. Zou, Joule **3**, 1140 (2019).

[14] M.A. Pan, T.K. Lau, Y. Tang, Y.C. Wu, T. Liu, K. Li, M.C. Chen, X. Lu, W. Ma, and C. Zhan, J. Mater. Chem. A **7**, 20713 (2019).

[15] L. Meng, Y. Zhang, X. Wan, C. Li, X. Zhang, Y. Wang, X. Ke, Z. Xiao, L. Ding, R. Xia, H.-L. Yip, Y. Cao, and Y. Chen, Science **361**, 1094 (2018).

[16] Z. Yao, H. Wu, Y. Li, J. Wang, J. Zhang, M. Zhang, Y. Guo, and P. Wang, Energy Environ. Sci. **8**, 3192 (2015).

[17] Z. Xiao, X. Jia, D. Li, S. Wang, X. Geng, F. Liu, J. Chen, S. Yang, T.P. Russell, and L. Ding, Sci. Bull. **62**, 1494 (2017).

[18] Z. Xiao, X. Jia, and L. Ding, Sci. Bull. **62**, 1562 (2017).

[19] F. Liu, Z. Zhou, C. Zhang, J. Zhang, Q. Hu, T. Vergote, F. Liu, T.P. Russell, and X. Zhu, Adv. Mater. **29**, 1606574 (2017).

[20] X. Li, F. Yu, S. Stappert, C. Li, Y. Zhou, Y. Yu, X. Li, H. Ågren, J. Hua, and H. Tian, ACS Appl. Mater. Interfaces **8**, 19393 (2016).

[21] W. Jiang, Y. Li, and Z. Wang, Chem. Soc. Rev. **42**, 6113 (2013).

[22] Z. Yao, X. Liao, K. Gao, F. Lin, X. Xu, X. Shi, L. Zuo, F. Liu, Y. Chen, and A.K.Y. Jen, J. Am. Chem. Soc. **140**, 2054 (2018).

[23] X. Huang, X. Liu, K. Ding, and S.R. Forrest, Mater. Horizons (2019).

[24] J.-Q. Xi, J.K. Kim, E.F. Schubert, D. Ye, T.-M. Lu, S.-Y. Lin, and J.S. Juneja, Opt. Lett. **31**,

601 (2006).

[25] M. Slootsky and S.R. Forrest, Opt. Lett. **35**, 1052 (2010).

Figure Captions

Figure 1. (a) Thin film absorption of PM6 and SFT8-4F used in the visible-absorbing sub-cell. (b) Thin film absorption of PCE-10, BT-CIC and BEIT-4F used in the ternary near-infrared absorbing sub-cell.

Figure 2. (a) Photoluminescence of PCE-10:BT-CIC:BEIT-4F blends at different blend ratios. (b) Electroluminescence (EL) spectrum of 1:1.5 PCE-10:BT-CIC binary cell, with Gaussian peaks fit (dashed lines) and their sum (blue line). (c) EL spectrum of 1:1.5 PCE-10:BEIT-4F with fits as in (b). (d) EL spectrum of 1:1.25:0.5 PCE-10:BT-CIC:BEIT-4F with fits as in (b).

Figure 3. (a) Current density-voltage (*J*-*V*) characteristics under 1 sun, AM1.5G simulated illumination and (b) external quantum efficiency (*EQE*) spectra of ternary cells with different PCE-10:BT-CIC:BEIT-4F blend ratios. (c) Open-circuit voltage (V_{OC}) and fill factor (*FF*) with different BEIT-4F blend ratio.

Figure 4. (a) Tandem device structure with optimized layer thicknesses and corresponding simulated optical field intensity distribution. (b) *J*-*V* characteristics of single-junction and tandem devices. (c) *EQE* of single-junction and tandem cells. The symbols are for discrete single-junction devices, whereas the dashed and solid lines are for sub-cells in the stack and their sum, colors represent the same sub-cells as in (b).

Figure 1.

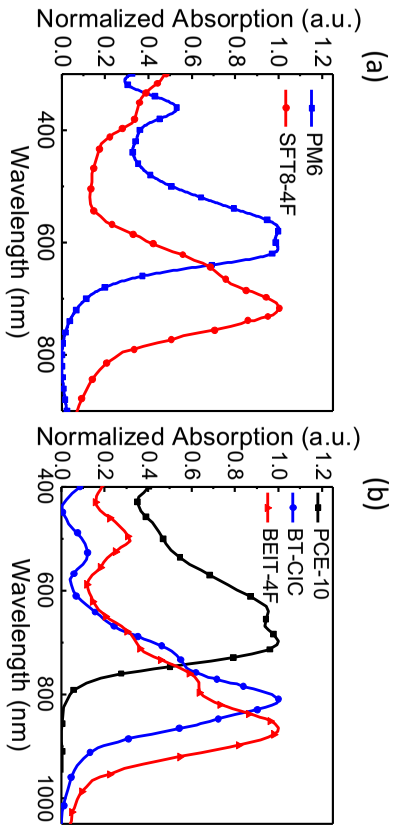

Figure 2.

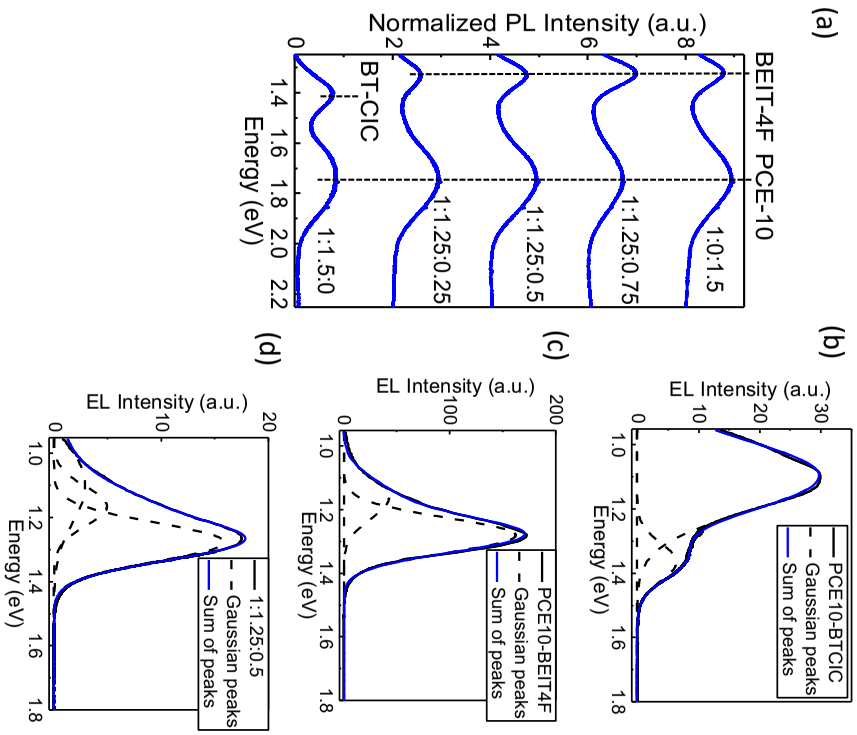

Figure 3.

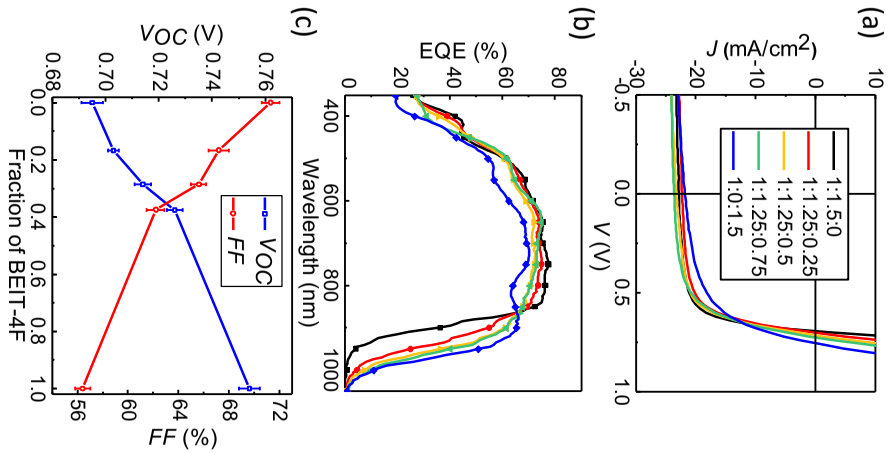

Figure 4.